Characterization of Endothelial Cilia Distribution During Cerebral-Vascular Development in Zebrafish (*Danio rerio*)

Shahram Eisa-Beygi, Fatiha M. Benslimane, Suzan El-Rass, Shubhangi Prabhudesai, Mahmoud Khatib Ali Abdelrasoul, Pippa M. Simpson, Huseyin C. Yalcin, Patricia E. Burrows, Ramani Ramchandran

Objective—Endothelial cells (ECs) sense and respond to flow-induced mechanical stress, in part, via microtubule-based projections called primary cilia. However, many critical steps during vascular morphogenesis occur independent of flow. The involvement of cilia in regulating these stages of cranial vascular morphogenesis is poorly understood because cilia have not been visualized in primary head vessels. The objective of this study was to investigate involvement of cilia in regulating the early stages of cranial vascular morphogenesis.

Approach and Results—Using high-resolution imaging of the *Tg(kdrl:mCherry-CAAX)*^{y171}*;(bactin::Arl13b:GFP)* zebrafish line, we showed that cilia are enriched in the earliest formed cranial vessels that assemble via vasculogenesis and in angiogenic hindbrain capillaries. Cilia were more prevalent around the boundaries of putative intravascular spaces in primary and angiogenic vessels. Loss of cardiac contractility and blood flow, because of knockdown of cardiac troponin T type 2a (*tnnt2a*) expression, did not affect the distribution of cilia in primary head vasculature. In later stages of development, cilia were detected in retinal vasculature, areas of high curvature, vessel bifurcation points, and during vessel anastomosis. Loss of genes crucial for cilia biogenesis (*ift172* and *ift81*) induced intracerebral hemorrhages in an EC-autonomous manner. Exposure to high shear stress induced premature cilia disassembly in brain ECs and was associated with intracerebral hemorrhages.

Conclusions—Our study suggests a functional role for cilia in brain ECs, which is associated with the emergence and remodeling of the primary cranial vasculature. This cilia function is flow-independent, and cilia in ECs are required for cerebral-vascular stability.

Visual Overview—An online visual overview is available for this article. **(*Arterioscler Thromb Vasc Biol*. 2018;38:2806-2818. DOI: 10.1161/ATVBAHA.118.311231.)**

Key Words: arteriovenous malformations ■ brain ■ cilia ■ endothelial cells ■ morphogenesis ■ shear stress ■ zebrafish

Before formation of a blood-brain barrier, the primary head vasculature in both teleosts and mammals assemble from a naive plexus through the migration and coalescence of angioblasts into a well-defined architecture.[1,2] This de novo process, also defined as vasculogenesis, occurs independent of blood flow. After vessel perfusion, a more elaborate system of vasculature emerges via angiogenesis, a process involving the sprouting of vessels from existing vasculature.[3] These newly formed capillaries help nourish the developing neural cells, thus are crucial for the development of the central nervous system (CNS).[4] Defects in the assembly, patterning, and lumenization of cranial vasculature can lead to abnormal vessel connections, loss of vessel integrity, intracranial aneurysms, and deterioration of neurons. Hence, identifying mediators of early cranial vascular assembly is instrumental in elucidating the etiology of developmental vascular pathologies in the brain.

See accompanying editorial on page 2763
See cover image

The primary cilium is a microtubule-based sensory organelle protruding from the apical surfaces of most eukaryotic cells. In endothelial cells (ECs), the cilium is specialized to sense and transduce flow-induced mechanical input into structural and functional changes in EC shape and behavior.[5] A single primary cilium in ECs projects into the vascular lumen and is connected, via the basal body, to cytoskeletal elements.[6,7] The contribution of cilia to early and flow-independent aspects of cranio-vascular morphogenesis and patterning have hitherto been unreported. Emerging studies in zebrafish and mice suggest that loss of components of cilia biogenesis disrupt cerebral-vascular integrity, as evidenced by intracranial hemorrhages (ICH) and intracranial aneurysms.[8–10] Consistently, clinical research suggests increased

Received on: April 23, 2018; final version accepted on: September 5, 2018.

From the Department of Radiology (S.E.-B., P.E.B.), Division of Neonatology, Department of Pediatrics (S.P., P.M.S., R.R.), and Department of Obstetrics and Gynecology (R.R.), Medical College of Wisconsin, Milwaukee; Biomedical Research Center, Qatar University, Doha (F.M.B., M.K.A.A., H.C.Y.); and Institute of Medical Science, University of Toronto, Ontario, Canada (S.E.-R.).

The online-only Data Supplement is available with this article at https://www.ahajournals.org/doi/suppl/10.1161/ATVBAHA.118.311231.

Correspondence to Patricia Burrows, MD, Medical College of Wisconsin, 9000 W Wisconsin Ave, MS7 721, Milwaukee, WI 53226, email pburrows@chw.org or Ramani Ramchandran, PhD, Children's Research Institute, Medical College of Wisconsin, 8701 Watertown Plank Rd, Milwaukee, WI 53226, email rramchan@mcw.edu

Nonstandard Abbreviations and Acronyms	
BA	basal artery
CNS	central nervous system
CtAs	central arteries
ECs	endothelial cells
hpf	hours postfertilization
ICH	intracranial hemorrhage
IFT	intraflagellar transport
MO	morpholino oligonucleotide
PHBC	primordial hindbrain channel
PMBC	primordial midbrain channel

risk of intracranial aneurysm ruptures in patients with autosomal dominant polycystic kidney disease, an inherited ciliopathy condition. However, the potential contribution of endothelial cilia to aneurysms in autosomal dominant polycystic kidney disease patients remains elusive.[11–13] In support of cilia involvement in vascular stabilization, a recent zebrafish study has demonstrated that pharmacological and genetic ablation of ciliary function impairs flow-mediated mural cell recruitment in vivo.[14] Taken together, these emergent studies in different model systems suggest a functional role for cilia in regulating cerebral-vascular stability. However, to date, there has been no systematic study of cilia distribution during the formation, remodeling, and maturation of the cranial vascular network. To this end, we performed high-resolution imaging of tissue-specific transgenic reporter lines to characterize the distribution of cilia in nascent brain ECs, with a focus on the emergence of primary vascular plexus and the arteriovenous connections in the hindbrain. Additionally, we used loss- and gain-of-function studies, along with increased shear stress, to determine the contribution of cilia to brain vascular stability.

Materials and Methods

The authors declare that all supporting data are available within the article (and in the online-only Data Supplement).

Zebrafish Husbandry, Transgenic, and Mutant Strains

The following zebrafish lines were used in this study: Tübingen (ZIRC [Zebrafish International Resource Center], Eugene, Oregon), *Tg(fli1:EGFP)*^{y1} [1], *Tg(fli1a:nEGFP)*^{y7} [15] (*Tg(gata1:dsRed)*^{sd2},[15] *Tg(bact::Arl13b-GFP)*,[16] *Tg(kdrl:mCherry-CAAX)*^{y171}[3] and *ift172*^{hi2211}[9]. Adult fish were maintained under a constant temperature of 28.0°C and were subjected to 14-hour light: 10-hour dark photoperiod at the Children's Research Institute and Midwest Athletes Against Childhood Cancer Fund Fish facilities. All animal studies performed in these facilities were under Medical College of Wisconsin–approved protocol Animal Use Application 320. Measurements for flow velocity and shear stress were performed at Qatar University's Biomedical Research Center. All relevant fish husbandry and handling protocols were approved by Qatar University's Institutional Animal Care and Use Committee. All fish were handled according to standard husbandry protocols.[17] Freshly fertilized embryos were procured through natural breeding of adult zebrafish and were kept at 28.0°C in 1X E3 embryo medium (E3 medium) containing 5 mmol/L NaCl, 0.17 mmol/L KCl, 0.33 mmol/L $CaCl_2$, 0.33 mmol/L $MgSO_4$, and 0.05% methylene blue. In some instances, embryos were treated with 0.003% of 1-phenyl-2-thiourea (Sigma-Aldrich), starting at 24 hours postfertilization (hpf), to minimize pigmentation.

Morpholino Oligonucleotides

An antisense morpholino oligonucleotide (MO) targeting the translation-start site (ATG) of *ift81* (MO:*ift81*^{ATG}) was designed to knockdown the expression of *ift81*.[9] To halt cardiac contractions and fluid flow, we designed a MO targeting the ATG translation-start site of cardiac troponin T type 2a, *tnnt2a* (*MO:tnnt2a*^{ATG}). As a negative control, we used a standard control MO (control-MO) specific to a human β-globin intron mutation. All MO solutions were synthesized by GeneTools (Oregon). The MO sequences are as follows:

MO:*ift81*^{ATG}: 5'-CGATAAATTTAAGCTGTTCGCTCAT-3'
MO:*tnnt2a*^{ATG}: 5'-CATGTTTGCTCTGATCTGACACGCA-3'
Control-MO: 5'-CCTCTTACCTCAGTTACAATTTATA-3'

All MO solutions were briefly heated at 65°C and resuspended in 1X Danieau buffer (58 mmol/L NaCl, 0.7 mmol/L KCl, 0.4 mmol/L MgSO4, 0.6 mmol/L $Ca(NO_3)_2$, 5.0 mmol/L HEPES, pH 7.6), and 0.1% (w/v) phenol red dye (Sigma-Aldrich), to a final concentration of 8 ng/nL. Embryos at 1 to 2 cell stage were positioned in individual grooves made on a 1.0% agarose gel and were initially injected at concentrations ranging from 0.5 to 6 ng/nL.

Endothelial-Specific ift81 Rescue Construct

The *kdrl:eGFP-2A-ift81* rescue construct was provided by Brant Weinstein Lab (National Institutes of Health). In the rescue construct, the EC-specific promoter, *kdrl*, drives the expression of the *eGFP-2a-ift81* fusion protein. The ATG start site of *ift81* has been modified such that some of the bases in the MO target sequence were replaced with synonymous nucleotides that do not change protein sequence. Specifically, the wild type, 5'-ATGAGCGAACAGCTTAAATTTATC-3', had been changed to 5'-ATGAG*T*GA*G*CA*AT*TAAA*G*TT*C*AT*T*-3'. The circular plasmid was resuspended in Tris-EDTA buffer (10 mmol/L Tris, pH 8, 01 mmol/L EDTA, pH 8), diluted to a final concentration of 40 ng/μL in 1X Danieau buffer, containing 0.1 % (w/v) phenol red dye. The plasmid was coinjected with 2 ng MO:*ift81*^{ATG} into 1-cell stage *Tg(kdrl:mCherry-CAAX)*^{y171} embryos at concentrations of 10 to 30 ng/μL. Embryos with transient eGFP (enhanced green fluorescent protein) expression in CNS blood vessels were then scored for presence or absence of ICH at 48 hpf.

Genomic DNA Extraction, Real-Time Polymerase Chain Reaction, and Sequencing

To genotype the *ift172*^{hi2211} retroviral insertional mutants, total genomic DNA was extracted from wild-type and potentially mutant fish, using 50 mmol/L NaOH and 1M Tris-HCl, pH 8.0, as described before.[18] A real-time polymerase chain reaction, involving primers flanking the insertion site was performed. The primers used for real-time polymerase chain reaction were

2211 C: 5'-GATGGAGCTGCTAAAGTCACCTG-3'
nLTR3 (viral element-specific reverse primer): 5'-CTGTT CCATCTGTTCCTGAC-3'

Sequencing was performed to verify insertion site, using the CEQ-8000 Genetic Analysis System and the aforementioned pair of primers.

Confocal Microscopy

For confocal microscopy, transgenic embryos, at various developmental stages, were embedded in 1% low melting agarose in E3 medium and 30 μg/mL tricaine mesylate (ethyl 3-aminobenzoate methanesulfonate; Sigma-Aldrich) for immobilization. Embryos were mounted on 35 mm glass-bottom Petri dishes (CELLVIS) and multiple Z-stacks were taken with a Zeiss LSM 510 AxioImager. All fluorescent image data were collected using Carl Zeiss LSM 510 laser scanning microscopy (Jena, Germany) equipped with a plan-apochromat ×20/0.8 numerical aperture (NA) lens. Images were collected (pinhole set at 1 airy unit) with appropriate dichroics and filters for each fluorescent protein. Image pixel saturation was corrected with photomultiplier tube detector gain and offset controls, as per the manufacturers' recommendations. Projections of summed Z-stacks

and enhancement of brightness and contrast were adjusted using Fiji software (National Institutes of Health).

Bright-Field/Fluorescent Microscopy

For bright-field/fluorescent microscopy and time-lapse analyses, wild-type or transgenic embryos were first embedded in 1% low melting agarose in E3 medium and 30 µg/mL tricaine mesylate. Embryos were mounted on 35 mm glass-bottom Petri dishes and imaged using Keyence BZ-X700 fluorescent microscope (Japan). A Texas Red filter cube (OP-87765, Keyence) was used to detect mCherry and dsRed (red fluorescent protein)-labeled cells, a GFP filter cube (OP-87763, Keyence) was used to detect GFP/EGFP-labeled tissues, and a 4′,6-diamidino-2-phenylindole (DAPI) filter cube (OP-87762, Keyence) was used to image DAPI-stained samples. Z-series bright-field and fluorescent images were acquired, and composite images were generated using the BZ-X Image Analyzer software. Brightness and contrast were adjusted using Fiji Software.

Whole-Mount In Situ Hybridization

Whole-mount in situ hybridization was performed as described.[19] A digoxigenin-labeled *pdgfrb* mRNA probe was synthesized from pJC-53.2-pdgfrb plasmid,[20] provided by Bruce Appel lab (University of Colorado). An in vitro transcription reaction mixture containing the polymerase chain reaction product amplified from pJC-53.2-pdgfrb (using T7 primers), 10x digoxigenin RNA labeling mix (Roche) and SP6 RNA polymerase (MEGAscript) were combined and incubated for ≈2 hours at 37°C to synthesize the antisense probe. Any residual DNA was then digested using TURBO DNase (Invitrogen), and the probe was purified using lithium chloride (LiCl) precipitation. After whole-mount in situ hybridization, embryos were mounted in 1% low melting agarose and imaged using a Nikon NBZ 1500 dissecting microscope, equipped with a Nikon DXM 1200 C digital camera.

Whole-Mount DAPI Staining

At 24 hpf, the *Tg(fli1a:nEGFP)*^{y7}*;(bactin:Arl13b:GFP)* embryos were fixed in 4% paraformaldehyde/1X PBS with Tween 20 overnight and incubated in 100 µg/mL of DAPI (Sigma-Aldrich) solution for 5 minutes to counterstain the nEGFP (nuclear enhanced green fluorescent protein)-labeled EC nuclei. Embryos were washed in 1X PBS with Tween 20 and imaged using Keyence BZ-X700 fluorescent microscope.

Measurement of PMBC Blood Flow Velocity, Shear Stress, and Pulse

For measurement of blood-flow velocity in the primordial midbrain channels (PMBCs), 33 hpf embryos (at either 28°C or 34.5°C) were stabilized in 3% methylcellulose and visualized using Zeiss SteREO Discovery V8 Microscope, equipped with Hamamatsu Orca Flash high-speed camera and a workstation equipped with HCImage software. For each embryo, a 10-s bright-field video of the head was recorded at 100 frames per second at a magnification of ×150. The same region in the PMBC was localized to measure the flow velocity, PMBC pulse, and PMBC diameter, using MicroZebralab application (v3.6; ViewPoint, France; Figure XI in the online-only Data Supplement). Shear stress was calculated using the formula below, where µ is the blood viscosity (dynes/cm^2), V is the average blood velocity (µm/s), and D is the vessel diameter (µm).[21]

$$\tau = \frac{4\mu V_{mean}}{D}$$

Statistical Analysis

For the assessment of the percentage of total cilia in the PMBC that reach a length of 3 to 5 µm at different stages of development, N=6 distinct embryos were used corresponding to each developmental stage; mean values±SDs were plotted (Figure VB in the online-only Data Supplement). Groups were compared using ANOVA, and a post hoc Tukey honestly significant difference (HSD) analysis was performed. Normality was checked with a Kolmogorov-Smirnov test (P>0.2), and all but data at 32 hpf (P<0.009) were normally distributed. Thus, in addition, nonparametric analysis using a Kruskal-Wallis test and a Mann-Whitney test was also performed. Irrespective, there was a difference overall, P≤0.001. Data at 24 and 26 hpf were different than each other and from data at 28 hpf. Statistics were done using IBM SPSS Statistics 24 software. For endothelial-specific rescue experiment, data were analyzed using a Mann-Whitney test on an IBM SPSS Statistics 24 software, P<0.001. For flow-related data sets (Figure 5A), statistical analysis was performed using GraphPad Prism 6 software. Distribution was investigated using D'Agostino and Pearson omnibus normality test. Depending on the distribution, data were analyzed using Student t test or a Mann-Whitney test. A P value of <0.05 was considered statistically significant. For data showing percentage of embryos with ICH at different temperature conditions (Figure 5L), the percentage of embryos with ICH were analyzed as a 2-ANOVA with factors: temperature (28°C, 32.5°C, or 34.5°C) and background of fish (wild-type, *ift172*^{hi221}, MO:*ift81*^{ATG} injected). A post hoc analysis was done using Tukey HSD. Normality was assumed because of the small sample size (N=3 experiments) for the groups.

Results

Ciliation of Primary Head Vasculature Precedes Cardiac Contractions and Blood Flow and Is Associated With Vascular Lumen Formation In Vivo

In zebrafish, the primary cranial vasculature assembles from a naïve plexus, independent of fluid flow.[1,2] To determine cilia distribution in this rudimentary network of ECs, we intercrossed several tissue-specific transgenic reporter lines. The *Tg(kdrl:mCherry-CAAX)*^{y171} line, in which the CAAX prenylation motif enables red fluorescent labeling of EC membranes, helps mark the outline of ECs surrounding the vascular spaces.[3] The *Tg(fli1a:nEGFP)*^{y7} line allows for nuclear localization of EGFP in ECs.[22] The *Tg(fli1:EGFP)*^{y1} line marks all ECs, and the *Tg(gata1:dsRed)*^{sd2} line expresses dsRed in primitive erythrocytes.[15] Finally, the *Tg(bactin:Arl13b:GFP)* strain in which mouse Arl13b (ADP ribosylation factor-like GTPase 13B), a small GTPase expressed in ciliary axoneme, is fused to GFP and driven under ubiquitous β-actin promoter activity[16,23] marks ciliary membranes.

By 24 hpf, the PMBC is the first major head vessel to assemble de novo (Figures I and IIA in the online-only Data Supplement).[4,24] The PMBC runs on either side of the vascular plan and provides venous drainage on flow induction through its posterior extension, the primordial hindbrain channel (PHBC; Figure IIB and IIC in the online-only Data Supplement). At 24 hpf, the PMBC is not fully lumenized but composed of multiple intravascular spaces of variable sizes that together form an irregularly shaped structure (Figure 1A–1C). Confocal microscopy of the double transgenic *Tg(kdrl:mCherry-CAAX)*^{y171}*;(bactin::Arl13b:GFP)* line at 24 hpf revealed that GFP-positive cilia were enriched throughout the length of vessel, with ≈18.6 cilia per PMBC (SD ±3.1; N=8 fishes). Most cilia were concentrated around the boundaries of intravascular spaces lining the PMBC (64.7%; SD ±9.3%; N=8 fishes; Figure 1D–1F and Figure IID–IIG in the online-only Data Supplement).

To confirm the endothelial origin of these cilia, we crossed the EC nuclei marker, *Tg(fli1a:nEGFP)*^{y7}, with the *Tg(bactin:Arl13b:GFP)* line. At 24 hpf, we observed 1 cilium per EC nuclei (Figure 1G–1J) and further that most cilia were

distributed around the edges of and projecting into the budding intravascular spaces (Figure 1G–1I). Counterstaining of nEGFP-labeled EC nuclei with the blue-fluorescent nuclear stain, DAPI, revealed that 74% ECs in the PMBC harbored primary cilia (SD ±9.2%, N=8 fishes) at 24 hpf (Figure III in the online-only Data Supplement). Time-lapse imaging revealed that these cilia exhibited rapid changes in conformation despite absence of fluid flow. (Movies I and II in the online-only Data Supplement). Through time-lapse imaging, we observed that the spontaneous beating of cilia was concurrent with the directional migration of EC nuclei in the PMBC (Figure 1J). To gain further insights into the functional outcome of ciliary dynamics, we used the double transgenic *Tg(kdrl:mCherry-CAAX)* ^{y171}*;(bactin::Arl13b:GFP)* line and observed that the beating motion of cilia before flow inception was accompanied by progressive expansion or enlargement of intravascular spaces circumscribed by mCherry-CAAX expression (Figure 1K).

Next, to confirm that the emergence and distribution pattern of cilia in primary head vasculature preceded both flow induction and the mechanical stretch (pulsation) generated by cardiac contractions, we used an antisense MO-based approach to knockdown the expression of cardiac troponin T type 2a (*tnnt2a*) in *Tg(kdrl:mCherry-CAAX)* ^{y171} embryos. Loss of *tnnt2a* impairs sarcomere assembly and induces a reproducible silent heart phenotype.[7] In zebrafish, myocardial contractions begin as early as 24 hpf, although brain vessels are not perfused until 28 hpf. Injection of 0.5 to 2 ng of *tnnt2a* MO into freshly fertilized *Tg(kdrl:mCherry-CAAX)* ^{y171}*;(bactin::Arl13b:GFP)* embryos produced a noncontractile phenotype in 100% of embryos at 24 to 28 hpf (n=87 embryos; Figure IVA–IVC and Movies III and IV in the online-only Data Supplement). At 24 hpf, the *tnnt2a*-MO-injected embryos manifested cilia in the PMBCs and these cilia were mostly aligned around the intravascular spaces before lumen formation (Figure IVD and IVE in the online-only Data Supplement). This agrees with the observations made by Goetz et al,[7] who showed that cilia continue to persist in zebrafish trunk artery in *tnnt2a* mutants and that these cilia are structurally similar to their wild-type counterparts. Thus, these results suggest that the emergence and subcellular localization of cilia in newly formed head vessels are independent of both cardiac contractions and blood flow and that cilia dynamics contribute to vascular lumen formation in a flow-independent manner.

By 28 hpf, as the PMBC adopted a continuous and hollow tubular conformation just before perfusion, most cilia were observed to be projecting from the apical surfaces of the vessel wall and protruding into the newly formed vascular lumen (89.4% facing lumen; SD ±9.3%; N=8 fishes; Figure 1L–1N). At 32 hpf, as the PMBC was fully perfused, primary cilia continued to persist under physiological flow conditions (Figure 1O). Changes in cilia length could be observed in real-time, as early as 24 hpf (Figure VA in the online-only Data Supplement), with most cilia in the PMBCs reaching a maximum length of 3 to 5 µm by 28 hpf, just before perfusion (77.5% cilia with length of 3–5 µm; SD ±10.3%; N=6 fishes; $P<0.001$, Student t test and post hoc Tukey HSD; Figure VB in the online-only Data Supplement). To confirm that on perfusion, physiological blood flow elicits ciliary bending, we used the doubly transgenic *Tg(gata1:dsRed)*^{sd2}*;(bactin::Arl13b:GFP)* line to simultaneously label primitive erythrocyte lineages and cilia. Time-lapse imaging, at the onset of flow, revealed that endothelial cilia in the PMBCs bend on contact with dsRed-labeled erythrocytes (Figure VC in the online-only Data Supplement). In contrast, cessation of flow, by exposure to 100 µg/mL of tricaine mesylate, stopped the directional bending of cilia (Figure VD in the online-only Data Supplement). These results suggest that cilia that emerge before flow persist during vessel perfusion and are responsive to physiological flow.

Primary Cilia Are Expressed During Hindbrain Angiogenesis

We next investigated whether cilia were expressed in later-forming angiogenic capillaries that start penetrating the hindbrain region following flow inception. In zebrafish, shortly after the formation of a primary cranial network and following perfusion, angiogenic mechanisms are activated in the hindbrain, with the first wave of sprouts originating from the PHBCs between 33 hpf and 40 hpf.[3] By 33 hpf, central arteries (CtAs) start to emerge from the dorsal surfaces of the PHBCs, in the form of tip cells, migrate dorsa-medially, and align at the midline (Figure VIA–VID in the online-only Data Supplement; Figure 3A and 3B). Once there, the CtAs form connections with their adjacent neighbors and some fuse with the basal artery (BA) at the midline to connect the PHBCs to BA, thus, forming the earliest arteriovenous connections in the brain (Figure VIE and VIF in the online-only Data Supplement).[3] With the anastomosis of adjacent perfused CtAs, a complete circulatory loop is usually established by 55 to 60 hpf.[3] We next investigated which sequential steps in CtA formation are mediated by blood flow by observing CtA formation in *tnnt2a* morphants that lacked circulatory flow. Although cessation of flow did not affect the sprouting and anastomosis of CtAs or the formation of CtA-mediated arteriovenous connections between the PHBCs and the BA, these vessels did not remain patent and appeared thinner, when compared with those in control MO-injected embryos (Figure VII in the online-only Data Supplement). This suggests that CtA sprouting and anastomosis are independent of flow or cardiac contractions but that CtAs require perfusion to remain patent.

Next, we examined the distribution of cilia during these defined stages of hindbrain angiogenesis by imaging the *Tg(kdrl:mCherry-CAAX)* ^{y171}*;(bactin::Arl13b:GFP)* line. Starting at 33 hpf, we noted that the CtA sprouts originating from the dorsal walls of the PHBC harbor cilia as they migrate dorsomedially (Figure 2C, 2D, and 2J). By 40 hpf, as most CtA sprouts reached the dorsal medial boundary and displayed a prominent lumen, cilia were specifically distributed around the boundaries of these emergent intravascular spaces (Figure 2E–2G). We detected cilia at both the base and tip of the CtA sprouts, where prominent intravascular spaces had started to emerge (Figure 2G). At 55 hpf, primary cilia were detected as a perfused circulatory loop was established between the 2 adjacent CtAs (Figure 2H and 2I), as well as in the CtA-mediated arteriovenous connections formed between the PHBCs and the BA (Figure VIII in the online-only Data Supplement). Collectively, these observations suggest that endothelial cilia are expressed during both flow-independent

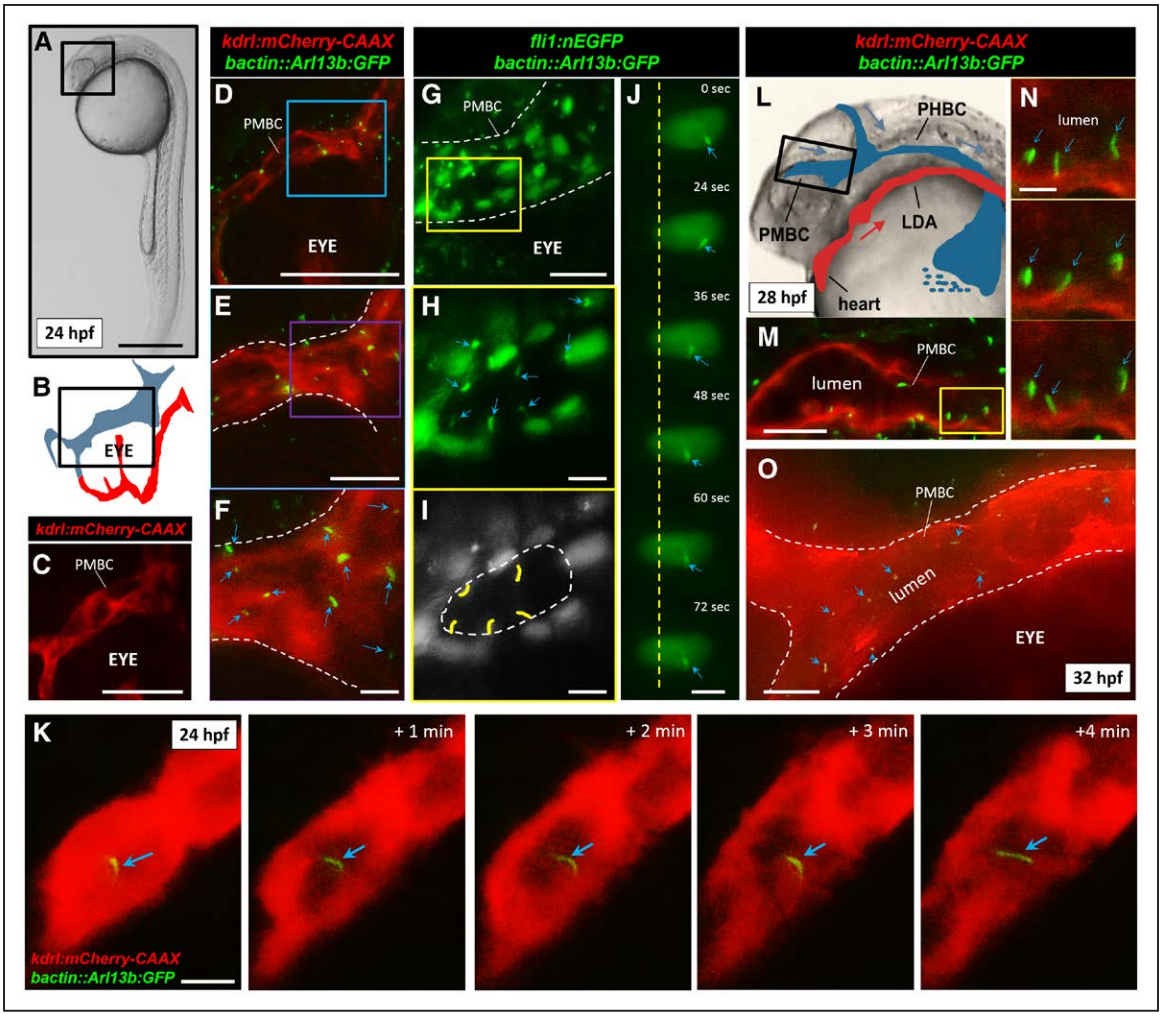

Figure 1. Characterization of primary cilia distribution in primordial cerebral vessels. **A**, Transmitted light microscopy image of a 24 h postfertilization (hpf) zebrafish embryo, lateral view. Scale bar: 200 µm. **B**, Schematic diagram of the cranial vascular anatomy of the boxed region. Veins are depicted in blue and arteries are shown in red. Not to scale. **C**, Confocal image of the region of interest in *Tg(kdrl:mCherry-CAAX)*^{y171} showing the primordial midbrain channel (PMBC). Scale bar: 40 µm. Eye is labeled for reference. **D**–**F**, Confocal microscopic images of the PMBC in the double transgenic *Tg(kdrl:mCherry-CAAX)*^{y171}*;(bactin::Arl13b:GFP)* line at 24 hpf, n=14 embryos. Scale bar: 40 µm. **E** and **F**, Higher magnification photomicrographs of the regions of interest in the PMBC. Blue arrows denote GFP (green fluorescent protein)-labeled primary cilia. PMBC outlines are marked by dashed lines. Scale bars: 20 and 10 µm, respectively. **G**, Confocal microscopic image of part of PMBC in the double transgenic *Tg(fli1a:nEGFP)*^{y7}*;(bact::Arl13b-GFP)* line at 24 hpf, n=6 embryos. PMBC outlines are marked by dashed lines. Scale bar: 20 µm. **H**, Higher magnification photomicrographs of the region of interest. Primary cilia are denoted by blue arrows. Scale bar: 5 µm. **I**, Pseudo-coloring of the region of interest is shown. Primary cilia are highlighted in yellow color. Putative intravascular space is marked by dashed lines. Scale bar: 5 µm. **J**, Stills from time-lapse fluorescent microscopy of the *Tg(fli1a:nEGFP)*^{y7}*;(bact::Arl13b-GFP)* double transgenic embryo at 24 hpf, showing a single endothelial cell (EC) nuclei (GFP) and associated cilium (GFP). Blue arrow designates the cilium. Yellow vertical dashed line is placed to confirm EC nuclei displacement over time. Scale bar: 5 µm. **K**, Stills from time-lapse fluorescent microscopy of the double transgenic 24 hpf *Tg(kdrl:mCherry-CAAX)*^{y171}*;(bact::Arl13b-GFP)* fish, showing endothelial cilium in relation to intravascular space in the anterior part of PMBC. Blue arrows point to cilium. Scale bar: 10 µm. **L**, Transmitted light microscopy image of a representative 28 hpf zebrafish embryo, showing schematic depiction of arteries (red) and veins (blue) in the head. **M**, Confocal microscopic image of the boxed region, showing a fully lumenized PMBC in the double transgenic *Tg(kdrl:mCherry-CAAX)*^{y171}*;(bact::Arl13b-GFP)* embryo before flow inception. Scale bar: 10 µm. **N**, Stills from time-lapse confocal microscopy of the designated region at a higher magnification, showing cilia dynamics over time. Blue arrows point to cilia. Scale bar: 5 µm. **O**, Confocal microscopic image of the PMBC in the double transgenic *Tg(kdrl:mCherry-CAAX)*^{y171}*;(bact::Arl13b-GFP)* line at 32 hpf, following flow inception. PMBC outlines are marked by dashed lines. Blue arrows point to cilia. Scale bar: 10 µm. All images are presented with anterior to left and posterior to right. LDA indicates lateral dorsal aorta; and PHBC, primordial hindbrain channel.

and flow-mediated stages of hindbrain angiogenesis, as newly formed sprouts migrate, anastomose, and establish a perfused circulatory loop between the BA and the PHBCs.

Endothelial Cilia Are Confined to a Subset of Embryonic, Larval, and Juvenile CNS Vasculature

Primary cilia in ECs disassemble under high flow and shear stress conditions in vitro; an observation suggesting that cilia are specialized to detect lower magnitudes of flow regimes.[5,25,26] Interestingly, in zebrafish, heart rate increases with gestational age, resulting in linear increases in flow velocity and shear stress through embryogenesis and early larval development.[27,28] Consistently, Goetz et al[7] have shown that by 48 hpf, endothelial cilia are almost completely abrogated in zebrafish trunk and caudal vasculature, concomitant with increases in flow velocity and shear stress levels. This suggested that cilia are dispensable in more mature zebrafish blood vessels. However, whether cilia continue to persist

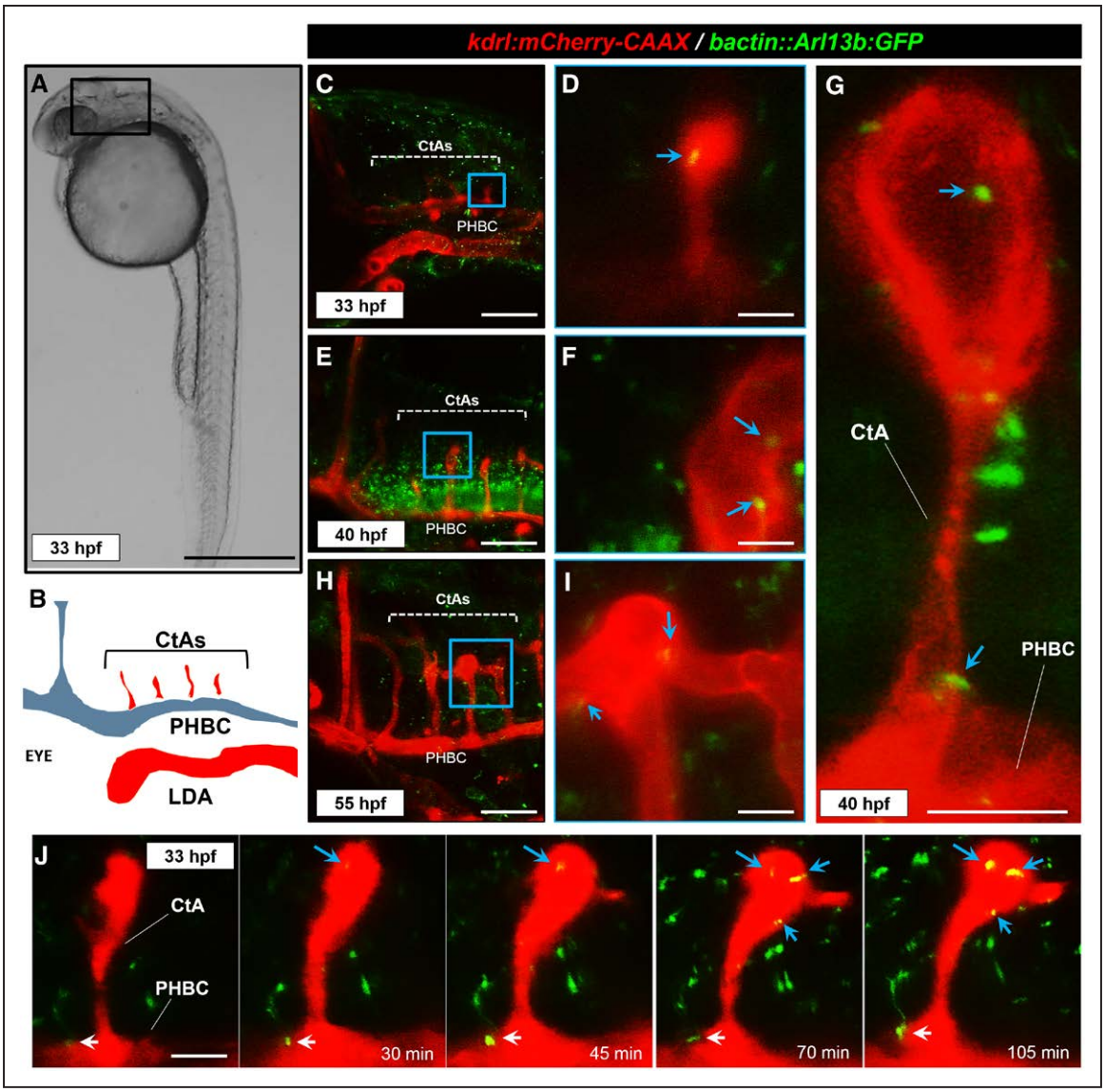

Figure 2. Primary cilia are detected in angiogenic hindbrain vasculature. **A**, Transmitted light image of a representative 33 h postfertilization (hpf) zebrafish embryo, lateral view. Scale bar: 200 μm. **B**, Schematic diagram of the hindbrain cranial vascular anatomy of the boxed region. Not to scale. Arteries are depicted in red and veins are shown in blue. **C**, Confocal image of the hindbrain vasculature in the double transgenic *Tg(kdrl:mCherry-CAAX)*^{y171}*;(bact::Arl13b-GFP)* line at 33 hpf. Central arteries (CtAs) and the primordial hindbrain channel (PHBC) are labeled. Scale bar: 100 μm. **D**, Higher magnification of the designated area in **C** showing single CtA sprout. Blue arrow denotes primary cilium. Scale bar: 5 μm. **E**, Confocal image of the hindbrain vasculature at 40 hpf. Scale bar: 100 μm. **F**, Higher magnification of the designated area in **E** showing tip of a single CtA sprout. Cilia (shown by blue arrows) are specifically found around the boundaries of emerging intravascular spaces. Scale bar: 10 μm. **G**, Representative confocal image of a CtA sprout at 40 hpf, showing emergence of intravascular lumens and cilia deposition at the tip and stalk ends of the sprout. Blue arrows point to primary cilia marking the edges of the intravascular spaces. Scale bar: 10 μm. **H**, Confocal image of part of the hindbrain vasculature at 55 hpf. Scale bar: 100 μm. **I**, Higher magnification of the designated are in **H**, showing anastomosis of 2 ipsilateral CtA sprouts. Blue arrows denote cilia. Scale bar: 10 μm. **J**, Time-lapse confocal images of a single CtA sprout at different stages of development. White arrow designates primary cilium on PHBC, and blue arrows show primary cilia associated with CtA. Scale bar: 10 μm. All images are presented with anterior to left and posterior to right.

in more mature CNS vessels was unknown. To address this, we performed confocal microscopy on the *Tg(kdrl:mCherry-CAAX)* ^{y171}*;(bactin::Arl13b:GFP)* double transgenic line during embryonic (2 days postfertilization), larval (4 and 6.5 days postfertilization), and juvenile (30 days postfertilization) stages of development. High-resolution imaging revealed that although most of the vascular cilia had disappeared, a subset of vessels in the CNS continued to retain their primary cilia, predominantly, in retinal vasculature (Figure 3A–3C), in curved, and arch-shaped brain vessels (Figure 3D–3F), during the process of vessel anastomosis (Figure 3G–3I) and at vessel bifurcation or branching points (Figure 3J–3L). These results suggest that cilia continue to persist in a subset of cranial and ocular vascular beds that present with nonlinear contours and topographies during embryonic, larval, and, juvenile stages.

Loss of Proteins Associated With Anterograde Cilia Transport Induces Intracerebral Hemorrhage in an EC-Autonomous Manner

Our observations suggest that cilia in brain ECs are responsible for cerebral-vascular development. In agreement with

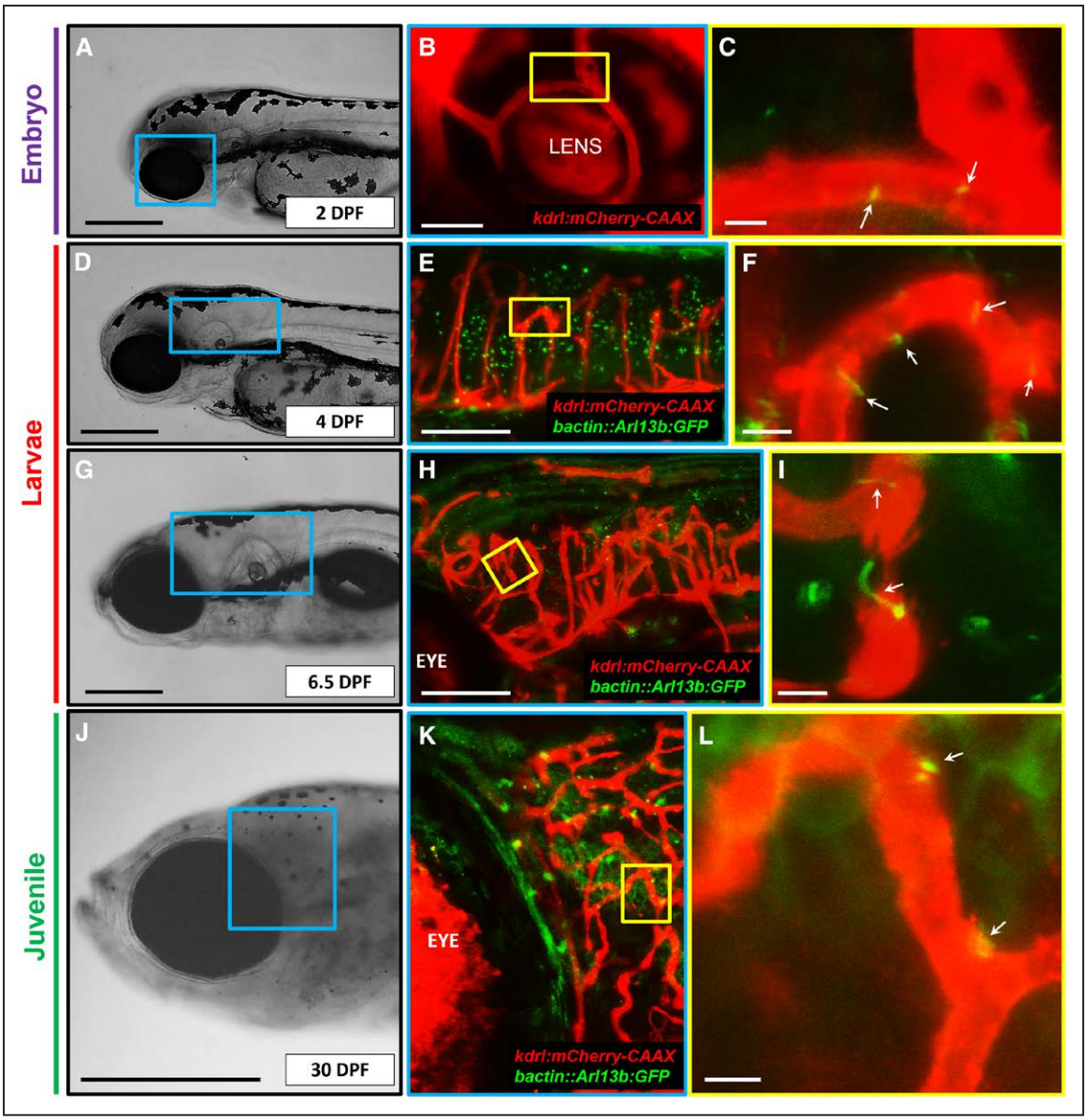

Figure 3. Endothelial cilia are confined to a subset of embryonic, larval, and juvenile central nervous system vasculature. **A**, Transmitted light image of a representative 2 d postfertilization (DPF) zebrafish embryo head, with magnified image of blue boxed region shown in B. Scale bar: 200 µm. **B**, Confocal image of the region of interest (blue box) in the *Tg(kdrl:mCherry-CAAX)*^{y171} embryo, showing part of the retinal vasculature. **C**, Higher magnification of the region designated by yellow box, showing cilia deposition (GFP [green fluorescent protein], appears yellow because of colocalization) in the lumenal compartments of retinal vasculature (mCherry-CAAX). White arrows denote primary cilia. Scale bar: 5 µm. **D**, Transmitted light image of a representative 4 DPF zebrafish larva head, with magnified image of blue boxed region shown in **E**. Scale bar: 200 µm. **E**, Confocal image of the region of interest (blue box) in the *Tg(kdrl:mCherry-CAAX)*^{y171}*;(bact::Arl13b-GFP)* line. **F**, Higher magnification of the region designated by yellow box, showing cilia enrichment in curved vasculature. White arrows denote primary cilia. Scale bar: 5 µm. **G**, Transmitted light image of a representative 6.5 DPF zebrafish larva head with magnified image of blue boxed region shown in **H**. Scale bar: 200 µm. **H**, Confocal image of the region of interest (blue box in **G**) in the *Tg(kdrl:mCherry-CAAX)*^{y171}*;(bact::Arl13b-GFP)* line at higher magnification. **I**, Higher magnification of the region defined by yellow box, showing cilia in vessels undergoing anastomosis. **J**, Transmitted light image of a representative 30 DPF zebrafish head, with a blue boxed region shown magnified in **K**. Scale bar: 1 mm. **K**, Confocal image of the region of interest (blue box in **J**) in the *Tg(kdrl:mCherry-CAAX)*^{y171}*;(bact::Arl13b-GFP)*line. Yellow box is magnified in **L**. **L**, Higher magnification of the region of interest (yellow box in **K**), showing cilia deposition (blue arrows) at vessel branching points. Scale bar: 5 µm. All images are lateral and presented with anterior to left and posterior to right.

our observations, recent studies in zebrafish and mice suggest that loss of components of cilia biogenesis lead to loss of cerebral-vascular integrity.[8–10] To investigate this hypothesis, we used 2 independent, but complementary, loss-of-function approaches. In the first approach, we investigated a previously identified genetic mutant carrying a retroviral insertion in the intraflagellar transport 172 (*ift172*) gene,[29] which encodes a subunit of the intraflagellar transport subcomplex IFT (intraflagellar transport)-B, necessary for ciliary assembly and maintenance[30] (Figure 4A). Consistent with previous observations in zebrafish models of ciliopathy, homozygous *ift172*^{hi2211} fish, although viable into early larval stages of development, displayed ventral body curvature in the posterior region by 48 to 52 hpf (Figure 4B and 4C).[31–33] An incross of heterozygous *ift172*^{hi2211} fish resulted in ≈11.8% of the embryos exhibiting cranial hemorrhages by

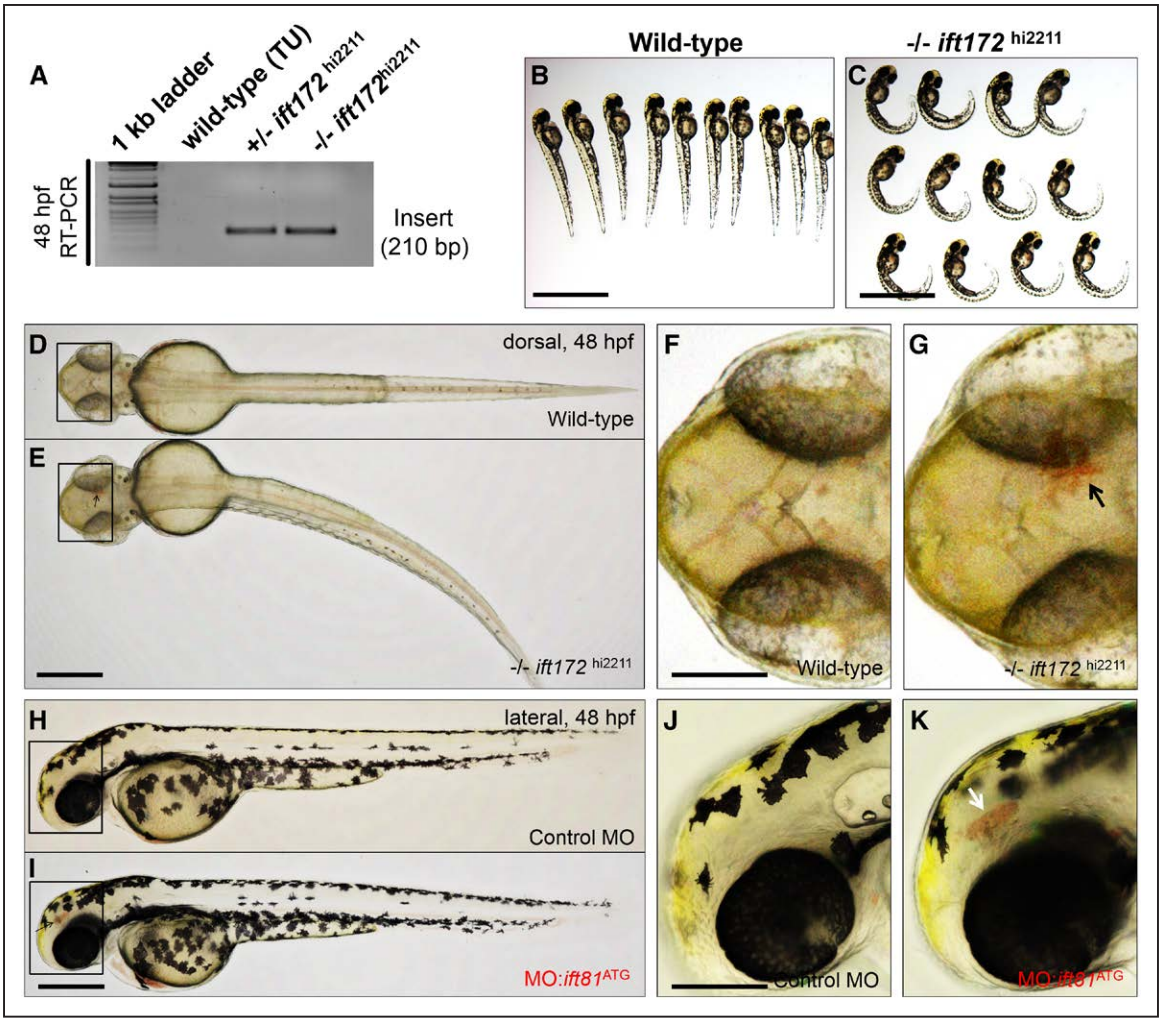

Figure 4. Loss of components of anterograde cilia transport induces intracranial hemorrhages in developing zebrafish. **A**, Real-time polymerase chain reaction (RT-PCR) mediated screen for 210 bp viral/insertion-specific amplicon in genomic DNA extracted from wild-type, heterozygous, and homozygous *ift172*^{hi2211} mutants. **B** and **C**, Bright-field images of representative wild-type and $^{-/-}$*ift172*^{hi2211} mutants at 48–52 h postfertilization (hpf) are shown. Scale bars: 500 μm. **D** and **E**, Representative dorsal views of whole-mount wild-type and $^{-/-}$*ift172*^{hi2211} zebrafish at 48–52 hpf. Scale bar: 200 μm. **F** and **G**, Higher magnification photomicrographs of the boxed regions in **D** and **E**. Black arrow denotes area of hemorrhage in the $^{-/-}$*ift172*^{hi2211} embryo. Anterior is to left. Scale bar: 100 μm. **H** and **I**, Representative lateral views of whole-mount embryos either injected with control morpholino oligonucleotide (control MO) or a MO targeting the ATG site of *ift81* (MO:*ift81*^{ATG}), imaged at 48–52 hpf. Scale bar: 200 μm. **J** and **K**, Higher magnification photomicrographs of the boxed regions in **H** and **I**. White arrow points to area of hemorrhage in the MO:*ift81*^{ATG}-injected embryo. Anterior is to left and posterior to right. Scale bar: 150 μm. TU indicates Tübingen.

48 to 52 hpf (SD ±1.9%; N=3 treatments; n>100 embryos/treatment; Figure 4D–4G), a phenotype which was previously noted.[9] In the second approach, we used a morpholino-based antisense strategy to target the translation-start site (ATG) of *ift81* (MO:*ift81*^{ATG}), which encodes another anterograde IFT gene in the IFT-B subcomplex.[34] Injection of ≈2 ng of MO:*ift81*$^{e3:i3}$ into freshly fertilized embryos resulted in 16.7% of embryos displaying cranial hemorrhages at 48 to 52 hpf (SD ±3.5%; N=3 treatments; n>130 embryos/treatment; Figure 4H–4K), compared with 0% (N=3 treatments; n>90 embryos/treatment) of embryos injected with a control MO targeting a human β-globin intron mutation. Injection of higher doses (>4 ng) of MO:*ift81*^{ATG} did not increase hemorrhage prevalence but resulted in hydrocephalus and ventral body curvature (Figure IX in the online-only Data Supplement). The low penetrance of ICH phenotype in *ift172*^{hi2211} mutants or *ift81*^{ATG} morphants may be because of residual cilia function because it has been demonstrated that both maternal and zygotic loss of anterograde IFT genes are needed to induce complete loss of cilia in embryonic zebrafish.[35]

To confirm that the ICH phenotype associated with MO:*ift81*^{ATG} injection is a consequence of EC-specific defects, we performed a genetic rescue experiment by transiently overexpressing *ift81* in ECs of embryos injected with MO:*ift81*^{ATG}. The *kdrl:eGFP-2A-ift81 rescue* plasmid was coinjected with MO:*ift81*^{ATG} into 1-cell stage *Tg(kdrl:mCherry-CAAX)* ^{y171} embryos (Figure XA–XC in the online-only Data Supplement). At ≈36 hpf, embryos were sorted for coexpression of GFP in mCherry-labeled ECs (Figure XD–XF in the online-only Data Supplement). Overexpression of endothelial-specific *ift81* significantly reduced the ICH prevalence from 16% (SD ±1.75%; N=3 treatments; n>120 embryos/treatment) in MO:*ift81*^{ATG}-injected

embryos to 5.65% (SD ±1.64%; N=3 treatments; n>100 embryos/treatment; $P<0.001$, Mann-Whitney U test). Collectively, these results suggest that endothelial cilia are required for cerebral-vascular stabilization, at least, during development.

Increased Flow Velocity and Shear Stress Induce Loss of Endothelial Cilia in the PMBCs and Is Associated With Intracerebral Hemorrhages

In cultured ECs, high shear stress leads to shedding or disassembly of cilia.[25,26] Accordingly, we postulated that an abrupt increase in heart rate and consequential surge in flow velocity and shear stress would induce premature loss of EC cilia in the developing CNS vasculature. In zebrafish, flow velocity can be increased by raising the ambient temperatures.[27,28] This adaptive physiological response in zebrafish, coupled with their wide-ranging thermal tolerance, enables us to easily increase flow velocity and shear stress by elevating incubation temperatures by a few increments, without eliciting heat shock.[36] To test our hypotheses, freshly fertilized embryos were raised at the optimum temperature of 28°C. At 28 hpf, corresponding to onset of flow in the head (Figure IIB in the online-only Data Supplement), these embryos were transferred to a 34.5°C incubator. Next, using a high-speed camera, we measured flow velocity (μm/s), shear stress (dynes/cm^2) and PMBC pulse (bpm) in these embryos (Figure XI in the online-only Data Supplement; See Measurement of PMBC blood flow velocity, shear stress and pulse in the Materials and Methods section). Consistent with our hypothesis, flow velocity, shear stress, and pulse values for PMBC increased significantly after 5 hours of incubation at 34.5°C (Figure 5A; Movies V and VI in the online-only Data Supplement). Next, we used the *Tg(kdrl:mCherry-CAAX)^{y171};(bactin::Arl13b:GFP)* double transgenic line to assess cilia distribution in these embryos. At 48 hpf, embryos raised at 28°C retained their cilia in the PMBC (Figure 5B and 5C). However, in embryos transferred to 34.5°C, we observed complete loss of cilia signal in the PMBCs but not in the adjacent tissues (N=8 embryos for each temperature; Figure 5D and 5E), suggesting that increased shear stress and flow velocity result in dissolution or disassembly of cilia in parts of the cranial vasculature. When raised to 48 to 52 hpf, ≈13% of the embryos raised at 34.5°C showed cranial hemorrhages (SD ±2.7%; N=3 treatments; n>100 embryos/treatment), compared with 1% of embryos raised at 28°C (SD ±1%; N=3 treatments; n>100 embryos/treatment). The loci and severity of hemorrhages varied but appeared to originate from the PMBCs (Figure 5F). Except for the ICH phenotype, embryos raised at 34.5°C were indistinguishable from those raised 28°C and did not display overt developmental defects, cardiotoxicity, or hemorrhages in other vascular beds (Figure 5G), suggesting that the effects are confined to head vasculature.

To address whether the hemorrhages were because of vascular leakage, we crossed the endothelial-specific *Tg(fli1:EGFP)^{y1}* line with the erythrocyte-specific *Tg(gata1:dsRed)^{sd2}* fish, which revealed extravasation of dsRed-labeled blood components from cranial arteries that emanate from the dorsal surfaces of PMBC, suggesting loss of vascular integrity (Figure 5H–5K). Raising the flow velocity/shear stress also resulted in higher prevalence of hemorrhages in both the *ift172^{hi2211}* mutants and *ift81* morphants, suggesting that loss or reduced expression of genes required for cilia biogenesis augments the risk for vascular rupture, especially in the wake of abrupt increases in shear stress levels (Figure 5L). Collectively, these results argue that an abnormal surge in shear stress and cardiac output during a specific development stage induces loss of cilia in specific CNS vessels, and this is associated with loss of cerebral-vascular stability in zebrafish.

Discussion

The emergence of the embryonic CNS vascular system, from a primitive plexus into an ordered network of perfused and stable vessels, requires timely and precise control over EC behavior and morphology. Many critical steps in cranial vascular remodeling occur before flow inception, which until now was difficult to discern. Further, endothelial cilia may have an integral role during these early remodeling events. Our observations here reveal 4 salient features of cilia in relation to brain vascular development.

First, we show that primary cilia are enriched in nascent cranial vessels preceding lumen formation, suggesting that there are intrinsic inputs that trigger ciliogenesis or adjust cilia size in these nascent vascular beds that are independent of hemodynamic stimuli. Much of work on EC cilia suggests a role in flow-mediated mechano-transduction.[37–39] However, the detection of primary cilia in newly emerging vascular beds, during both vasculogenesis and early stages of angiogenesis, suggests a function that is independent of their role as passive biomechanical sensors of fluid flow. Of importance, the specific enrichment of cilia around the boundaries of budding intravascular spaces in both primary vessels and angiogenic capillaries is suggestive of a contribution to endothelial lumen formation. This is also supported by the observation that the beating of cilia is associated with progressive expansion of intravascular spaces in vivo (Figure 1K). Not surprisingly, the small GTPases, CDC42 (cell division control protein 42 homolog) and RAC1 (Ras-related C3 botulinum toxin substrate 1), both of which are central regulators of endothelial lumen formation,[40–43] are also required for primary cilia biogenesis.[44–47] Both Cdc42 and Rac1 control microtubule dynamics, which are major structural components of cilia. A recent mouse study shows that endothelial cilia dysfunction impairs lumen formation in the retinal vasculature, which supports our hypothesis that cilia are involved in vascular lumen formation.[25] These observations suggest that cilia have yet-to-be discerned functions in the formation of a patent lumen in different vascular beds before flow inception, a hypothesis that is currently under investigation in our laboratory.

Secondly, our work suggests involvement of endothelial cilia in all stages of hindbrain angiogenesis (Figure 2A–2J), including when venous-derived arterial sprouts migrate, anastomose, and establish a perfused circulatory loop in the hindbrain region. Although the sprouting and migration of hindbrain CtAs occur after inception of circulation, blood flow is not a requirement for these processes, evidenced by the fact that embryos with a silent heart show properly patterned CtA sprouts. Hence, it remains unknown whether the

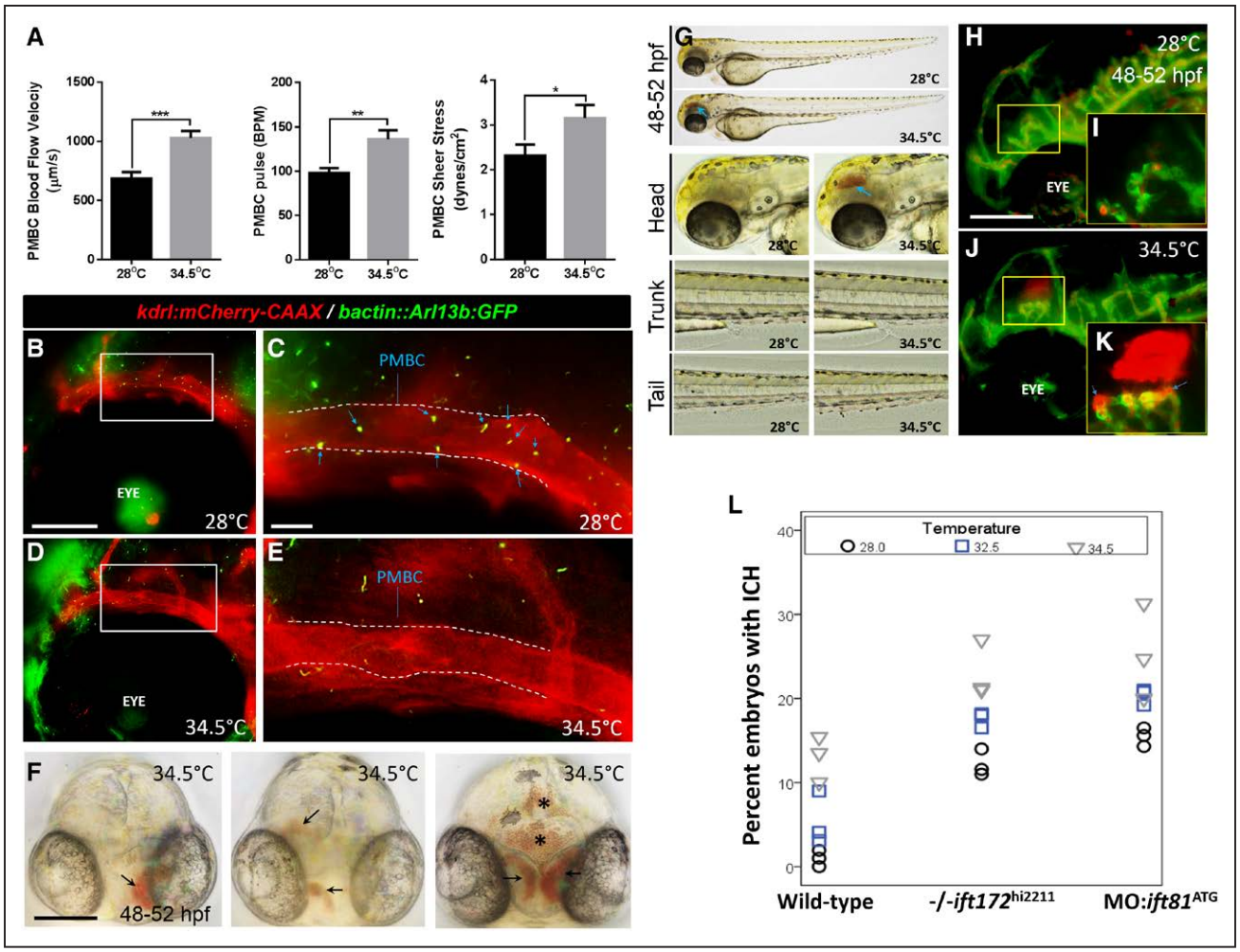

Figure 5. Increased flow velocity and shear stress disrupt cerebral-vascular stabilization, in part, via loss of endothelial cilia. **A**, Plots for primordial midbrain channel (PMBC) blood flow velocity (μm/s), pulse (bpm), and shear stress (dynes/cm^2) are shown. All data are represented as mean±SEM. Statistical analysis was performed using GraphPad Prism 6 software. Distribution was determined using D'Agostino and Pearson omnibus normality test. Parametric data were analyzed using Student *t* test while nonparametric data were analyzed using Mann-Whitney test. A *P* value of <0.05 was considered statistically significant. **P*<0.05, ***P*<0.001, and ****P*<0.0001 (N=10 embryos for 28°C and N=15 embryos 34.5°C groups, respectively). **B**, Maximum intensity projection of fluorescent z-stacks of the head region in a *Tg(kdrl:mCherry-CAAX)^{y171};(bact::Arl13b-GFP)* double transgenic zebrafish embryo maintained at 28°C. Scale bar: 40 μm. **C**, Higher magnification of the boxed region in **B**, showing cilia deposition in the PMBC. Blue arrows show primary cilia in the defined region of PMBC (outlined by dashed lines). Scale bar: 5 μm. Anterior is to left. **D**, Maximum intensity projection of fluorescent z-stack of the head region in a *Tg(kdrl:mCherry-CAAX)^{y171};(bact::Arl13b-GFP)* double transgenic zebrafish embryo maintained at 34.5°C. Scale bar: 40 μm. **E**, Higher magnification of the boxed region in **D**, with no primary cilia observed in the defined region of PMBC (outline by dashed lines). Scale bar: 5 μm. Anterior is to left. **F**, Representative frontal views of 48–52 h postfertilization (hpf) wild-type embryos raised at 34.5°C, showing multifocal hemorrhages with variable severities. Arrows point to regions of hemorrhage. Asterisks label regions of hematoma expansion into brain ventricles. Scale bar: 100 μm. **G**, Representative photomicrographs of wild-type embryos raised at 28°C or 34.5°C. Whole-body images, as well as higher magnifications of the head, trunk, and tail regions are shown. Blue arrow points to region of hemorrhage in the brain. Lateral images are shown. Anterior is to left. **H**, Maximum intensity projection of fluorescent z-stack of the head region in a *Tg(fli1:EGFP)^{y1};(gata1:dsRed)^{sd2}* double transgenic zebrafish embryo raised at 28°C and imaged at 48–52 hpf. Scale bar: 50 μm. **I**, Higher magnification of the yellow boxed region is shown. **J**, Maximum intensity projection of fluorescent z-stack of the head region in a *Tg(fli1:EGFP)^{y1};(gata1:dsRed)^{sd2}* double transgenic zebrafish embryo raised at 34.5°C and imaged at 48–52 hpf. **K**, Higher magnification of the yellow boxed region is shown. Hemorrhages are visible as extravasation of dsRed (red fluorescent protein)-labeled erythrocytes. Blue arrows indicate probable regions of vascular rupture. Lateral images are presented. Anterior is to left. **L**, Dot plots showing percentages of embryos (wild-type, *–/–ift172*^{hi221} and MO:*ift81*^{ATG} injected) presenting with intracerebral hemorrhages at 48–52 hpf after incubation in different ambient temperatures. All experiments for each temperature condition were repeated 3× (N=3 experiments), and data are presented as means for each experiment (n>100 embryos/treatment). Wild type differs from *–/–ift172*^{hi221} and MO:*ift81*^{ATG} injected embryos. For the MO:*ift81*^{ATG} group, wild-type embryos were injected with ≈2 ng of MO: *ift81*^{ATG} at 1-cell stage. The percent with intracranial hemorrhage (ICH) differs between temperatures. More information is provided in the Statistical Analysis of the Materials and Methods section.

contribution of cilia to hindbrain angiogenesis is in part or completely mediated via their flow-responsive function or if there are additional signaling pathways involving cilia that do not depend on flow. Consistent with our observations in hindbrain angiogenic vessels, studies in zebrafish and mice suggest that cilia are required for developmental angiogenesis of other vascular beds, including caudal vein plexus in zebrafish and retinal vasculature in mice.[7,25]

Thirdly, here, we show that EC cilia are also found in a subset of CNS vessels during larval and juvenile stages of development (Figure 3A–3L). These results contrast with those from Goetz et al,[7] who previously reported almost complete

loss of cilia beyond 48 hpf in the zebrafish trunk and caudal vasculature, suggesting that brain vessels, because of their contours and varying diameters, tend to sustain differential flow profiles and perhaps differential cilia deposition rates. In our analysis, we have observed a higher preponderance of cilia in curved and bifurcating regions of CNS vessels in larval or juvenile fish, although the functional relevance of this phenomenon is not known. These observations agree with those reported in mice, which show enriched cilia deposition in curved and branching regions of the aorta.[48,49] Curved and branching regions of aorta are considered atheroprone regions. Thus, whether the function of cilia and their distribution in these geometrically constrained vessels (compared to linear vessels) is because of differential flow regimes needs more insights.

Finally, inhibition of genes crucial for cilia biogenesis impairs cerebral-vascular integrity. Mutation or morpholino-induced loss of proteins involved in anterograde IFT, such as *ift172* and *ift81*, result in cranial hemorrhages. These results confirm previously reported association between loss of *ift* genes and intracerebral hemorrhages in zebrafish.[9]

Additionally, we have shown that a nonphysiological increase in flow velocity and shear stress, through a surge in ambient temperature during development, is inversely associated with primary cilia distribution in brain vessels and results in increased prevalence of ICHs in embryos. The temperatures we have used are below levels that would induce heat shock, given that the heat-shock promoter (*hsp701*) activity is induced at around 37°C.[36]

In this study, we have not investigated how the loss of endothelial cilia disrupts vascular stability, but we speculate that cilia are connected to cell-cell junctions via their intimate associations with the cytoskeletal elements. We posit that changes in cilia dynamics because of high shear stress would affect the adherence of ECs to one-another and to other cell types. If and how flow-induced loss of cilia affects cell-cell junctions needs to be explored in more detail.

Interestingly, hemorrhages were only confined to head vasculature and were not observed in the trunk or caudal vessels. This raises an intriguing question: Why are cranial vessels more prone to hemorrhage in response to abrupt increases in shear stress? In zebrafish, cardiac contractions begin at 24 hpf, and flow through trunk vessels starts concurrently (≈24–26 hpf), whereas head vessels are usually perfused at ≈28 hpf. Thus, a 4-hour delay in flow inception in the head appears consequential. We posit that during this 4-hour period, cilia in brain ECs are required for the assembly and organization of ECs into tubular structures. Hence, an abrupt increase in cardiac output at 28 hpf, may induce premature cilia disassembly during this period of dynamic vascular remodeling, which would impair downstream morphological processes, such as cell-cell junction formation, manifesting as loss of vessel integrity at 48 hpf. In the trunk or caudal ECs, the sudden increases in flow rates will likely induce cilia disassembly, as in head vessels, but the major trunk axial vessels, such as dorsal aorta or cardinal vein, are already assembled by this time, and thus subsequent downstream processes are not expected to be influenced, as evidenced by the fact that no hemorrhages are observed in these regions.

A second hypothesis emerging from recent work is that impaired cilia biogenesis delays subsequent recruitment of other cell types that are required for cerebral-vascular stabilization, such as pericytes and smooth muscle cells. This hypothesis is based on recent evidence which suggests that cilia are required for mural cell recruitment of arterial fated vessels in zebrafish.[14] Using a riboprobe against *pdgfrb* (a marker for pericytes),[20] we provide evidence here that *pdgfrb*-expression is detectable as early as 48 hpf, but appears negligible in primary head vasculature at early stages and is more prevalent by 96 hpf (Figure XII in the in the online-only Data Supplement). Other groups have shown, through live imaging of transgenic strains, that *pdgrfb*-expressing cells emerge as early as 36 hpf in the zebrafish hindbrain region.[50] Thus, whether hemorrhages arise because of defective perivascular recruitment in the hindbrain vessels requires further investigation.

In summary, our studies suggest a function for cilia in regulating the earliest stages of cerebral-vascular morphogenesis. Extensive clinical evidence suggests a link between ciliopathies and elevated risk of hemorrhage-prone intracranial aneurysms in patients,[11–13,51] although the mechanisms by which ciliopathies induce EC dysfunction or pathological vascular remodeling in the brain are unknown. Our studies here provide a framework to investigate such clinically-relevant questions.

Acknowledgments

We thank Dr Brian Ciruna (University of Toronto, Canada) for their gift of *Tg(bact::Arl13b-GFP)* line, Dr Zhaoxia Sun (Yale University School of Medicine) for their gift of *ift172*^{hi2211} mutants, Dr Bruce Appel (University of Colorado Anschutz Medical Campus) for their gift of pJC-53.2-pdgfrb plasmid, Dr Brant Weinstein for their gift of kdrl:eGFP-2a-ift81 rescue plasmid, Dr Suresh Kumar (Medical College of Wisconsin) for access to confocal microscopy, training, and troubleshooting, and Zain Zaki Salim Zakaria (Qatar University, Qatar) for embryo collection towards flow and shear stress measurements.

Sources of Funding

S. Eisa-Beygi is supported by funds from Kelleigh's Cause Foundation. R. Ramchandran is also supported by 1R01HL123338, and partly supported by funds from Women's Health Research Program at the Medical College of Wisconsin. S. Prabhudesai is supported by Department of Pediatrics, and Children's Research Institute funds to R. Ramchandran. H.C. Yalcin is supported by QNRF (Qatar National Research Fund), National Priority Research Program NPRP 10-0123-170222, and Qatar University internal funds QUUG-BRC-2017-3 and QUST-BRC-SPR\2017-1.

Disclosures

None.

References

1. Isogai S, Horiguchi M, Weinstein BM. The vascular anatomy of the developing zebrafish: an atlas of embryonic and early larval development. *Dev Biol*. 2001;230:278–301. doi: 10.1006/dbio.2000.9995
2. Gore AV, Monzo K, Cha YR, Pan W, Weinstein BM. Vascular development in the zebrafish. *Cold Spring Harb Perspect Med*. 2012;2:a006684. doi: 10.1101/cshperspect.a006684

3. Fujita M, Cha YR, Pham VN, Sakurai A, Roman BL, Gutkind JS, Weinstein BM. Assembly and patterning of the vascular network of the vertebrate hindbrain. *Development*. 2011;138:1705–1715. doi: 10.1242/dev.058776
4. Ulrich F, Ma LH, Baker RG, Torres-Vázquez J. Neurovascular development in the embryonic zebrafish hindbrain. *Dev Biol*. 2011;357:134–151. doi: 10.1016/j.ydbio.2011.06.037
5. Hierck BP, Van der Heiden K, Alkemade FE, Van de Pas S, Van Thienen JV, Groenendijk BC, Bax WH, Van der Laarse A, Deruiter MC, Horrevoets AJ, Poelmann RE. Primary cilia sensitize endothelial cells for fluid shear stress. *Dev Dyn*. 2008;237:725–735. doi: 10.1002/dvdy.21472
6. Jones TJ, Adapala RK, Geldenhuys WJ, Bursley C, AbouAlaiwi WA, Nauli SM, Thodeti CK. Primary cilia regulates the directional migration and barrier integrity of endothelial cells through the modulation of hsp27 dependent actin cytoskeletal organization. *J Cell Physiol*. 2012;227:70–76. doi: 10.1002/jcp.22704
7. Goetz JG, Steed E, Ferreira RR, Roth S, Ramspacher C, Boselli F, Charvin G, Liebling M, Wyart C, Schwab Y, Vermot J. Endothelial cilia mediate low flow sensing during zebrafish vascular development. *Cell Rep*. 2014;6:799–808. doi: 10.1016/j.celrep.2014.01.032
8. Lamont RE, Vu W, Carter AD, Serluca FC, MacRae CA, Childs SJ. Hedgehog signaling via angiopoietin1 is required for developmental vascular stability. *Mech Dev*. 2010;127:159–168. doi: 10.1016/j.mod.2010.02.001
9. Kallakuri S, Yu JA, Li J, Li Y, Weinstein BM, Nicoli S, Sun Z. Endothelial cilia are essential for developmental vascular integrity in zebrafish. *J Am Soc Nephrol*. 2015;26:864–875. doi: 10.1681/ASN.2013121314
10. Liu M, Zhao J, Zhou Q, Peng Y, Zhou Y, Jiang Y. Primary cilia deficiency induces intracranial aneurysm. *Shock*. 2018;49:604–611. doi: 10.1097/SHK.0000000000000961
11. Chapman AB, Rubinstein D, Hughes R, Stears JC, Earnest MP, Johnson AM, Gabow PA, Kaehny WD. Intracranial aneurysms in autosomal dominant polycystic kidney disease. *N Engl J Med*. 1992;327:916–920. doi: 10.1056/NEJM199209243271303
12. Pirson Y, Chauveau D, Torres V. Management of cerebral aneurysms in autosomal dominant polycystic kidney disease. *J Am Soc Nephrol*. 2002;13:269–276.
13. Rozenfeld MN, Ansari SA, Shaibani A, Russell EJ, Mohan P, Hurley MC. Should patients with autosomal dominant polycystic kidney disease be screened for cerebral aneurysms? *AJNR Am J Neuroradiol*. 2014;35:3–9. doi: 10.3174/ajnr.A3437
14. Chen X, Gays D, Milia C, Santoro MM. Cilia control vascular mural cell recruitment in vertebrates. *Cell Rep*. 2017;18:1033–1047. doi: 10.1016/j.celrep.2016.12.044
15. Yaniv K, Isogai S, Castranova D, Dye L, Hitomi J, Weinstein BM. Live imaging of lymphatic development in the zebrafish. *Nat Med*. 2006;12:711–716. doi: 10.1038/nm1427
16. Borovina A, Superina S, Voskas D, Ciruna B. Vangl2 directs the posterior tilting and asymmetric localization of motile primary cilia. *Nat Cell Biol*. 2010;12:407–412. doi: 10.1038/ncb2042
17. Lawrence C. Advances in zebrafish husbandry and management. *Methods Cell Biol*. 2011;104:429–451. doi: 10.1016/B978-0-12-374814-0.00023-9
18. Meeker ND, Hutchinson SA, Ho L, Trede NS. Method for isolation of PCR-ready genomic DNA from zebrafish tissues. *Biotechniques*. 2007;43:610, 612, 614. doi: 10.2144/000112619
19. Thisse B, Thisse C. In situ hybridization on whole-mount zebrafish embryos and young larvae. *Methods Mol Biol*. 2014;1211:53–67. doi: 10.1007/978-1-4939-1459-3_5
20. Wang Y, Pan L, Moens CB, Appel B. Notch3 establishes brain vascular integrity by regulating pericyte number. *Development*. 2014;141:307–317. doi: 10.1242/dev.096107
21. Yalcin HC, Amindari A, Butcher JT, Althani A, Yacoub M. Heart function and hemodynamic analysis for zebrafish embryos. *Dev Dyn*. 2017;246:868–880. doi: 10.1002/dvdy.24497
22. Guarani V, Deflorian G, Franco CA, et al. Acetylation-dependent regulation of endothelial Notch signalling by the SIRT1 deacetylase. *Nature*. 2011;473:234–238. doi: 10.1038/nature09917
23. Yu JA, Castranova D, Pham VN, Weinstein BM. Single-cell analysis of endothelial morphogenesis in vivo. *Development*. 2015;142:2951–2961. doi: 10.1242/dev.123174
24. Proulx K, Lu A, Sumanas S. Cranial vasculature in zebrafish forms by angioblast cluster-derived angiogenesis. *Dev Biol*. 2010;348:34–46. doi: 10.1016/j.ydbio.2010.08.036
25. Vion AC, Alt S, Klaus-Bergmann A, Szymborska A, Zheng T, Perovic T, Hammoutene A, Oliveira MB, Bartels-Klein E, Hollfinger I, Rautou PE, Bernabeu MO, Gerhardt H. Primary cilia sensitize endothelial cells to BMP and prevent excessive vascular regression. *J Cell Biol*. 2018;217:1651–1665. doi: 10.1083/jcb.201706151
26. Iomini C, Tejada K, Mo W, Vaananen H, Piperno G. Primary cilia of human endothelial cells disassemble under laminar shear stress. *J Cell Biol*. 2004;164:811–817. doi: 10.1083/jcb.200312133
27. Baker K, Warren KS, Yellen G, Fishman MC. Defective "pacemaker" current (ih) in a zebrafish mutant with a slow heart rate. *Proc Natl Acad Sci USA*. 1997;94:4554–4559.
28. Barrionuevo WR, Burggren WW. O2 consumption and heart rate in developing zebrafish (Danio rerio): influence of temperature and ambient O2. *Am J Physiol*. 1999;276(2 pt 2):R505–R513.
29. Lunt SC, Haynes T, Perkins BD. Zebrafish ift57, ift88, and ift172 intraflagellar transport mutants disrupt cilia but do not affect hedgehog signaling. *Dev Dyn*. 2009;238:1744–1759. doi: 10.1002/dvdy.21999
30. Engel BD, Ishikawa H, Wemmer KA, Geimer S, Wakabayashi K, Hirono M, Craige B, Pazour GJ, Witman GB, Kamiya R, Marshall WF. The role of retrograde intraflagellar transport in flagellar assembly, maintenance, and function. *J Cell Biol*. 2012;199:151–167. doi: 10.1083/jcb.201206068
31. Bujakowska KM, Zhang Q, Siemiatkowska AM, et al. Mutations in IFT172 cause isolated retinal degeneration and Bardet-Biedl syndrome. *Hum Mol Genet*. 2015;24:230–242. doi: 10.1093/hmg/ddu441
32. Ryan S, Willer J, Marjoram L, Bagwell J, Mankiewicz J, Leshchiner I, Goessling W, Bagnat M, Katsanis N. Rapid identification of kidney cyst mutations by whole exome sequencing in zebrafish. *Development*. 2013;140:4445–4451. doi: 10.1242/dev.101170
33. Li J, Sun Z. Qilin is essential for cilia assembly and normal kidney development in zebrafish. *PLoS One*. 2011;6:e27365. doi: 10.1371/journal.pone.0027365
34. Bhogaraju S, Cajanek L, Fort C, Blisnick T, Weber K, Taschner M, Mizuno N, Lamla S, Bastin P, Nigg EA, Lorentzen E. Molecular basis of tubulin transport within the cilium by IFT74 and IFT81. *Science*. 2013;341:1009–1012. doi: 10.1126/science.1240985
35. Borovina A, Ciruna B. IFT88 plays a cilia- and PCP-independent role in controlling oriented cell divisions during vertebrate embryonic development. *Cell Rep*. 2013;5:37–43. doi: 10.1016/j.celrep.2013.08.043
36. Duszynski RJ, Topczewski J, LeClair EE. Simple, economical heat-shock devices for zebrafish housing racks. *Zebrafish*. 2011;8:211–219. doi: 10.1089/zeb.2011.0693
37. Egorova AD, van der Heiden K, Poelmann RE, Hierck BP. Primary cilia as biomechanical sensors in regulating endothelial function. *Differentiation*. 2012;83:S56–S61. doi: 10.1016/j.diff.2011.11.007
38. Mohieldin AM, Zubayer HS, Al Omran AJ, Saternos HC, Zarban AA, Nauli SM, AbouAlaiwi WA. Vascular endothelial primary cilia: mechanosensation and hypertension. *Curr Hypertens Rev*. 2016;12:57–67.
39. Nauli SM, Kawanabe Y, Kaminski JJ, Pearce WJ, Ingber DE, Zhou J. Endothelial cilia are fluid shear sensors that regulate calcium signaling and nitric oxide production through polycystin-1. *Circulation*. 2008;117:1161–1171. doi: 10.1161/CIRCULATIONAHA.107.710111
40. Abraham S, Scarcia M, Bagshaw RD, et al. A Rac/Cdc42 exchange factor complex promotes formation of lateral filopodia and blood vessel lumen morphogenesis. *Nat Commun*. 2015;6:7286. doi: 10.1038/ncomms8286
41. Koh W, Mahan RD, Davis GE. Cdc42- and Rac1-mediated endothelial lumen formation requires Pak2, Pak4 and Par3, and PKC-dependent signaling. *J Cell Sci*. 2008;121(pt 7):989–1001. doi: 10.1242/jcs.020693
42. Kamei M, Saunders WB, Bayless KJ, Dye L, Davis GE, Weinstein BM. Endothelial tubes assemble from intracellular vacuoles in vivo. *Nature*. 2006;442:453–456. doi: 10.1038/nature04923
43. Norden PR, Kim DJ, Barry DM, Cleaver OB, Davis GE. Cdc42 and k-Ras control endothelial tubulogenesis through apical membrane and cytoskeletal polarization: novel stimulatory roles for GTPase effectors, the small GTPases, Rac2 and Rap1b, and inhibitory influence of Arhgap31 and Rasa1. *PLoS One*. 2016;11:e0147758. doi: 10.1371/journal.pone.0147758
44. Zuo X, Fogelgren B, Lipschutz JH. The small GTPase Cdc42 is necessary for primary ciliogenesis in renal tubular epithelial cells. *J Biol Chem*. 2011;286:22469–22477. doi: 10.1074/jbc.M111.238469
45. Choi SY, Chacon-Heszele MF, Huang L, McKenna S, Wilson FP, Zuo X, Lipschutz JH. Cdc42 deficiency causes ciliary abnormalities and cystic kidneys. *J Am Soc Nephrol*. 2013;24:1435–1450. doi: 10.1681/ASN.2012121236
46. Epting D, Slanchev K, Boehlke C, Hoff S, Loges NT, Yasunaga T, Indorf L, Nestel S, Lienkamp SS, Omran H, Kuehn EW, Ronneberger O, Walz G, Kramer-Zucker A. The Rac1 regulator ELMO controls basal body

migration and docking in multiciliated cells through interaction with Ezrin. *Development*. 2015;142:174–184. doi: 10.1242/dev.112250
47. Madhivanan K, Mukherjee D, Aguilar RC. Lowe syndrome: between primary cilia assembly and Rac1-mediated membrane remodeling. *Commun Integr Biol*. 2012;5:641–644. doi: 10.4161/cib.21952
48. Van der Heiden K, Hierck BP, Krams R, de Crom R, Cheng C, Baiker M, Pourquie MJ, Alkemade FE, DeRuiter MC, Gittenberger-de Groot AC, Poelmann RE. Endothelial primary cilia in areas of disturbed flow are at the base of atherosclerosis. *Atherosclerosis*. 2008;196:542–550. doi: 10.1016/j.atherosclerosis.2007.05.030
49. Dinsmore C, Reiter JF. Endothelial primary cilia inhibit atherosclerosis. *EMBO Rep*. 2016;17:156–166. doi: 10.15252/embr.201541019
50. Ando K, Fukuhara S, Izumi N, Nakajima H, Fukui H, Kelsh RN, Mochizuki N. Clarification of mural cell coverage of vascular endothelial cells by live imaging of zebrafish. *Development*. 2016;143:1328–1339. doi: 10.1242/dev.132654
51. Cagnazzo F, Gambacciani C, Morganti R, Perrini P. Intracranial aneurysms in patients with autosomal dominant polycystic kidney disease: prevalence, risk of rupture, and management. A systematic review. *Acta Neurochir (Wien)*. 2017;159:811–821. doi: 10.1007/s00701-017-3142-z

Highlights

The major findings of this study include

- Ciliation of primary head vasculature precedes cardiac contractions and blood flow and is associated with vascular lumen formation in vivo
- Primary cilia are detected during all stages of hindbrain angiogenesis.
- In more mature brain vessels, primary cilia are restricted to retinal vasculature, as well as to curved and bifurcating vascular beds.
- Loss of anterograde *ift* genes and increased shear stress disrupt cerebral-vascular stability, as evidenced by intracranial hemorrhages.